J. Fluid Mech. (2015), *vol.* 765, R3, doi:10.1017/jfm.2014.718

JFM RAPIDS
journals.cambridge.org/rapids



Shape dynamics and scaling laws for a body dissolving in fluid flow

Jinzi Mac Huang[1], **M. Nicholas J. Moore**[1,2] **and Leif Ristroph**[1,†]

[1]Applied Mathematics Laboratory, Courant Institute, New York University, New York, NY 10012, USA

[2]Department of Mathematics and Geophysical Fluid Dynamics Institute, Florida State University, Tallahassee, FL 32306, USA

(Received 28 October 2014; revised 1 December 2014; accepted 9 December 2014; first published online 26 January 2015)

While fluid flows are known to promote dissolution of materials, such processes are poorly understood due to the coupled dynamics of the flow and the receding surface. We study this moving boundary problem through experiments in which hard candy bodies dissolve in laminar high-speed water flows. We find that different initial geometries are sculpted into a similar terminal form before ultimately vanishing, suggesting convergence to a stable shape–flow state. A model linking the flow and solute concentration shows how uniform boundary-layer thickness leads to uniform dissolution, allowing us to obtain an analytical expression for the terminal geometry. Newly derived scaling laws predict that the dissolution rate increases with the square root of the flow speed and that the body volume vanishes quadratically in time, both of which are confirmed by experimental measurements.

Key words: boundary layers, geophysical and geological flows, mixing and dispersion

1. Introduction

A broad class of natural and industrial processes involve the recession of solid boundaries due to the action of flowing fluids. Examples include the corrosion (Heitz 1991), erosion (Ristroph *et al.* 2012; Moore *et al.* 2013), ablation (Feldman 1959; Verniani 1961), melting (Hao & Tao 2002) and dissolution (Garner & Grafton 1954; Hanratty 1981; Daccord & Lenormand 1987) of materials. Often, the surface morphologies that result from these processes reflect the nature of the flows present. For dissolution specifically, the effects of flow can be seen across many scales, from branched or scalloped mineral surfaces (Blumberg & Curl 1974; Daccord 1987; Daccord & Lenormand 1987; Meakin & Jamtveit 2010) to vast cave and tunnel networks found in karst landscapes (Ford & Williams 2007). By understanding the physical principles behind their development, such geological features might be used

† Email address for correspondence: ristroph@cims.nyu.edu

© Cambridge University Press 2015

https://doi.org/10.1017/jfm.2014.718 Published online by Cambridge University Press

to infer past environmental conditions. Furthermore, the same principles of flow-driven dissolution could be put to use in the chemical (Garner & Grafton 1954; Garner & Keey 1958; Linton & Sutherland 1960; Steinberger & Treybal 1960; Levich 1962; Jeschke, Vosbeck & Dreybrodt 2001; Colombani 2008; Mbogoro *et al.* 2011) and pharmaceutical industries (Nelson & Shah 1975; Grijseels, Crommelin & De Blaey 1981; Missel, Stevens & Mauger 2004; Dokoumetzidis & Macheras 2006; Bai & Armenante 2009), which rely on the incorporation of solid compounds into solutions within reactors and the human body.

As is clear from stirring sugar into coffee or tea, flows tend to speed up dissolution. Earlier efforts to understand the effect of flows have focused on phenomenological models that describe the bulk mass transfer rate for static surfaces (Garner & Keey 1958; Linton & Sutherland 1960; Steinberger & Treybal 1960; Nelson & Shah 1975; Grijseels *et al.* 1981; Missel *et al.* 2004). However, a complete account of the dissolution dynamics must include the mutual influence of the solid and fluid phases: the flow acts to modify the shape, which in turn alters the near-body flow, and so on. Here, we aim to understand this shape–flow feedback, or moving boundary problem, by establishing a clean experimental setting that is amenable to theoretical treatment.

2. Experimental shape dynamics

We focus on bodies of simple initial shapes dissolving within unidirectional flows, with the hope of distilling principles that apply more generally. In particular, bodies of size $a \sim 1$–10 cm made of hard candy are placed within water flows of speed $U_0 \sim$ 10–100 cm s^{-1}. These scales yield a high Reynolds number $Re = aU_0/\nu \sim 10^4$, where ν is the kinematic viscosity of water. Typical dissolving rates are 1 cm h^{-1}, indicating that the boundary motion is many orders slower than the flow speed. Specifically, amorphous solidified sugar – called hard candy in the USA or boiled sweets in the UK – is made by heating an 8:3:2 mixture by volume of table sugar (sucrose), light corn syrup and water to 302 F (150 °C) and casting within moulds. Dissolution occurs within a water tunnel with test section 15 cm × 15 cm × 43 cm. Speed is continuously monitored by a laser Doppler velocimeter, and temperature is kept at 28 ± 1 °C.

Considering first a spherical initial geometry, we find that dissolution sculpts a unique shape that bears signatures of the flow. In figure 1(*a*), we show a photograph of the body removed after 60 min of dissolution in a flow of speed 30 cm s^{-1}. The body is composed of a rounded front face, a facet that encircles the body and is bounded by two ridges, and a flattened back side. While the front has been polished smooth, both the facet and the back show surface irregularities, which are presumably associated with unsteady local flow. To visualize the flow field, we seed the water with microparticles (3M microbubbles), illuminate a plane with a laser sheet, and capture time-exposed photographs. The streakline photograph of figure 1(*b*) shows that the flow remains attached over the front surface of the body before separating at the leading ridge of the facet. As illustrated in the schematic of figure 1(*c*), the back sits within an unsteady wake, and the facet is associated with a quiescent region between separation and the wake. We also use shadowgraph imaging to visualize variations in the concentration of dissolved sugars (Garner & Hoffman 1961). The image of figure 1(*d*) shows that the separation streamline carries a high solute concentration, suggesting that dissolution along the front face is confined to a thin layer that is then swept off the body.

We capture the development of these surface features using time-lapsed photography and image analysis. The data of figure 2(*c*) show that the rounded face persists

https://doi.org/10.1017/jfm.2014.718 Published online by Cambridge University Press

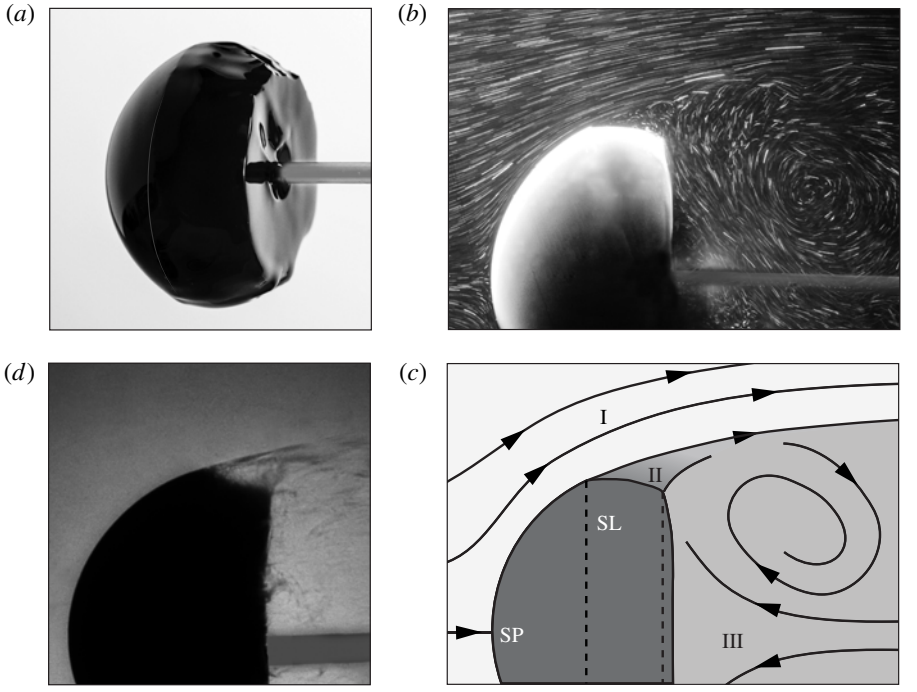


FIGURE 1. Dissolution of hard candy in flowing water. (*a*) The body starts as a sphere of diameter 6 cm, and the photograph shows the shape after 60 min of dissolution in a 30 cm s^{-1} flow (left to right). (*b*) Streaklines obtained by seeding the flow with microparticles. (*c*) Schematic showing the outer flow (I), quiescent (II) and wake (III) regions. The flow meets the body at the stagnation point (SP) and detaches at the separation line (SL). (*d*) Shadowgraph imaging shows that highly concentrated solution is swept off the body at the SL.

throughout the experiment, the back flattens relatively quickly, and the front and back surfaces approach one another, causing the intervening facet to shrink over time. The dynamics of the facet and the back appear to be closely related to the separated flow and wake region. The front surface, where flow is attached, experiences the highest dissolving rates and appears to be static in shape. However, careful inspection reveals that initial irregularities are smoothed over, suggesting that the rounded final shape is not simply a consequence of the initial shape. To test this idea, we consider a body that presents a flat wall to the flow, in particular a cylinder with one end facing upstream, as shown in figure 2(*b*), an arrangement that preserves axial symmetry. Interestingly, the front is rounded over time, as shown in figure 2(*d*). The emergence of this same final shape from different initial geometries suggests the existence of a stable attracting state for the fluid–structure dynamics.

The approach to this terminal state can be quantified by measuring how the dissolving rate varies both along the surface and at different times. In figure 2(*e*) we plot the normal velocity of the receding interface as a function of the arc length s along the spherical (top) and cylindrical (bottom) bodies. The rate is shown at early (red) and later (blue) times, and the arc length at which flow separation occurs is indicated by a vertical dashed line. For both geometries, the velocity is variable along the front surface for early times, indicating a change of shape. For the sphere,

https://doi.org/10.1017/jfm.2014.718 Published online by Cambridge University Press

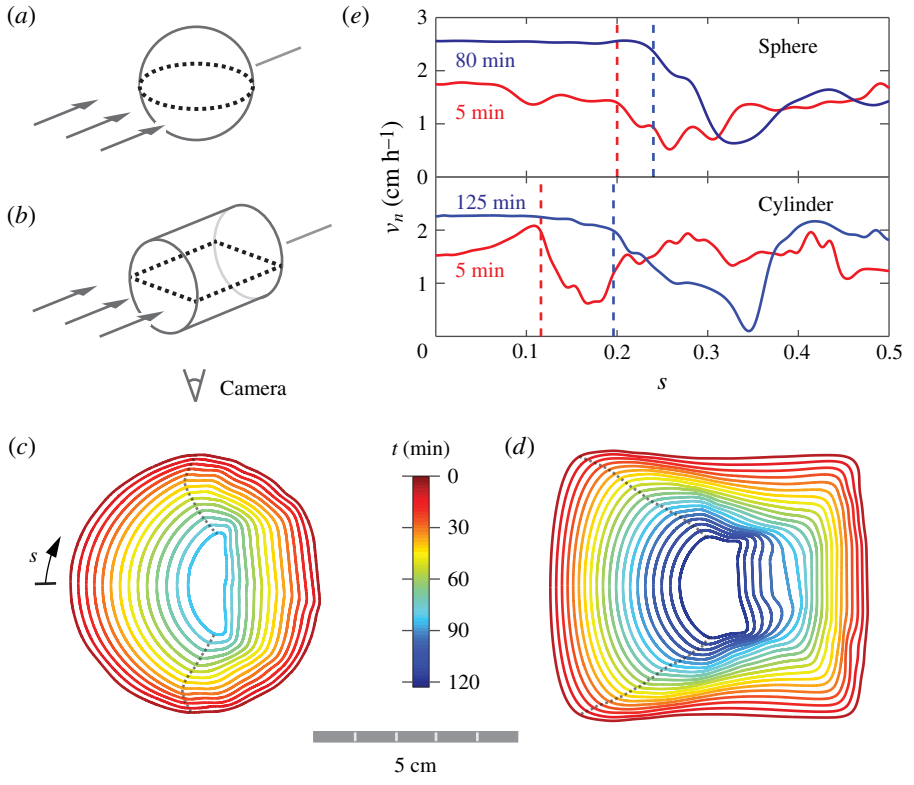


FIGURE 2. Shape evolution during dissolution. (*a,b*) Bodies of different initial shapes – a sphere and a cylinder with diameters of 6.0 and 6.9 cm, respectively – are presented with a flow of speed 30 cm s^{-1} and photographed from below. (*c,d*) Interfaces displayed every 6 min and colour-coded in time, with separation points indicated by the dotted line. (*e*) Comparison of the recession rate at locations along the body for the sphere (top) and cylinder (bottom) and at early (red) and late (blue) times. The arc length is 0 at the front and 0.5 at the back of the body, and separation is marked by dashed vertical lines.

these variations are slight and seem to be associated with manufacturing defects. For the cylinder, however, the rate is significantly lower near stagnation ($s = 0$) and higher at separation, which tends to round the initially flat face. In all cases, the rate along the front becomes more uniform at later times, thus tending to preserve the shape. Indeed, this self-similar recession is apparent from the even spacing between successive interfaces of figure 2(*c,d*) at later times.

3. Scaling laws

An understanding of these dynamics requires a model of how the concentration and flow fields affect dissolution. In the absence of flow, the solute simply diffuses and the boundary recedes at a rate given by Fick's law, $v_n = -D\partial c/\partial n$ (Garner & Suckling 1958; Garner & Hoffman 1961; Duda & Vrentas 1971). Here, D is the molecular diffusivity, c is the concentration of dissolved material and n is the surface normal. In the presence of flow, the washing away of solute tends to increase the concentration gradient and thus enhance the dissolution (Grijseels *et al.* 1981). Similar ideas hold

https://doi.org/10.1017/jfm.2014.718 Published online by Cambridge University Press

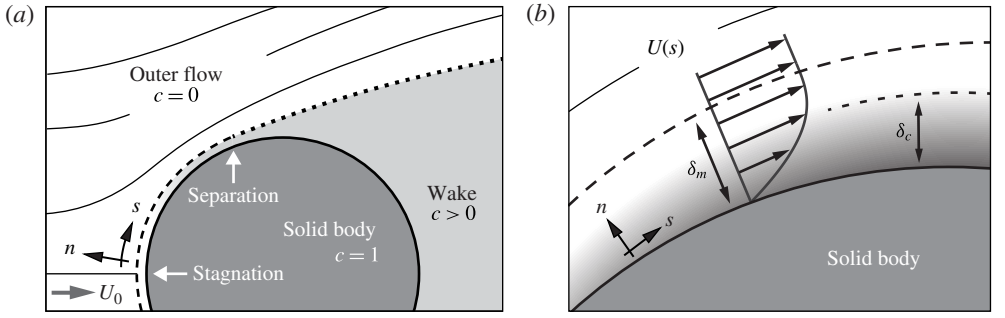


FIGURE 3. Schematics of the flow and concentration fields. (*a*) The steady outer flow consists of fresh water, while the attached flow near the body forms a boundary layer (dashed line) containing dissolved material. (*b*) Zoomed-in view of the momentum and concentration boundary layers (not to scale), the former defined by the flow velocity and the latter by the solute.

for forced thermal convection, where temperature is analogous to concentration and flow enhances the transfer of heat (Schlichting & Gersten 2000). For the mass transfer problem considered here, however, the flux of solute is associated with a change of shape and thus a change in the surrounding flow. As shown in figure 3(*a,b*), the attached flow along the front forms a momentum boundary layer of thickness δ_m in which the velocity rises from zero to a local outer flow value $U(s)$ (Childress 2009). Similarly, the dissolved material is confined to a concentration boundary layer of thickness δ_c (Schlichting & Gersten 2000). The arrangement of these layers depends on the relative importance of viscosity ν and diffusivity D, whose ratio is the Schmidt number $Sc = \nu/D$ (or Prandtl number Pr in thermal convection), and we estimate $Sc \sim 10^3$ in our experiments. Using an analogous relationship from thermal convection (Schlichting & Gersten 2000), we expect that $\delta_c/\delta_m \sim Sc^{-1/3} \sim 0.1$. Thus, high Sc indicates that viscosity dominates diffusion, and the solute is confined well within the flow boundary layer.

By considering how the boundary layer depends on the body size, we can incorporate the shape–flow interaction into scaling laws. For a flow of speed U_0 past a body of size a, the Prandtl boundary-layer equations indicate $\delta_m \sim \sqrt{\nu a/U_0}$ (Schlichting & Gersten 2000). On retaining only the dependence on a and U_0 and using $\delta_c \sim \delta_m$ from above, the interfacial velocity is then $v_n \sim 1/\delta_c \sim \sqrt{U_0/a}$. The body volume $V \sim a^3$ satisfies $\mathrm{d}V/\mathrm{d}t \sim v_n a^2 \sim \sqrt{U_0 V}$, and integration yields $V/V_0 = (1 - t/t_f)^2$, where V_0 is the initial volume and $t_f \sim {U_0}^{-1/2}$ is the total time to vanish. To assess these predictions, we use the measurements of figure 2(*c*) to extract volume over time, and figure 4(*a*) shows that the volume indeed vanishes quadratically in time. To test the relationship $t_f \sim {U_0}^{-1/2}$, we conduct experiments at different flow speeds and infer t_f from the measured volume dynamics. As shown in figure 4(*b*) and its inset, the time to vanish indeed scales with the flow speed as predicted. Further, these arguments indicate that the boundary layer thins as the body shrinks, which accounts for the greater v_n observed at later times, as shown in figure 2(*e*).

We note that these power laws can alternatively be derived through the scaling of the Sherwood number $Sh = a\partial c/\partial n$, which is defined to be the ratio of convective to diffusive material flux. In thermal convection, the Nusselt number Nu is analogous to the Sherwood number and measures the ratio of convective to conductive heat flux. Hence the well-known relationship for the thermal problem $Nu \sim Re^{1/2}Pr^{1/3}$ becomes

https://doi.org/10.1017/jfm.2014.718 Published online by Cambridge University Press

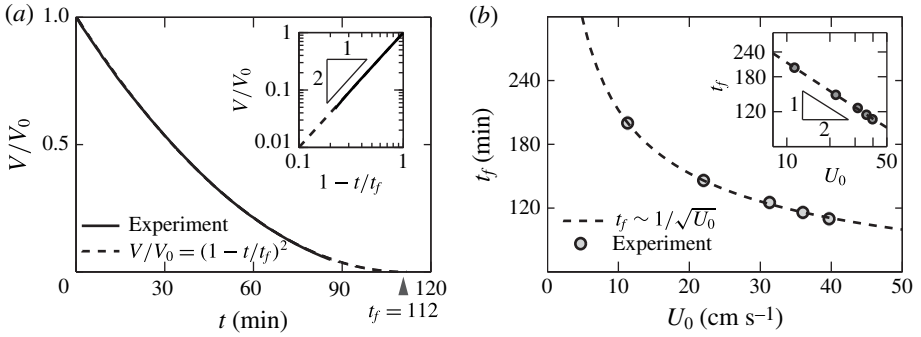


FIGURE 4. Scaling laws for dissolution in flow. (*a*) Decrease in volume over time for an initial sphere. Experimental measurements (solid curve) agree closely with the predicted power law (dashed curve). Inset: logarithmic-scale plot of normalized volume and time. (*b*) Total time to vanish as a function of flow speed for experiments (dots) and theory (dashed line). Inset: logarithmic-scale plot.

$Sh \sim Re^{1/2}Sc^{1/3}$ for our mass transfer problem. By the definition of the Sherwood number and Fick's law, and focusing on the dependence on a and U_0, we conclude that $Sh = a\partial c/\partial n \sim -av_n \sim Re^{1/2} \sim (aU_0)^{1/2}$, which leads to $v_n \sim U_0^{1/2}a^{-1/2}$ and gives the same scaling laws.

4. Two-dimensional theory for the terminal shape

To understand the terminal form seen in the experiments, we now extend our boundary-layer model to account for how the solute flux varies along the surface of the body. For this analysis, we are guided by the idea that uniform flux tends to preserve shape during dissolution (see figure 2*e*). Near stagnation, the flow accelerates as it deflects around the body, and the local outer flow takes the form $U(s) \propto s^{\alpha}$, where α depends on the geometry. Such flows are well-studied in thermal convection (Mahmood & Merkin 1988; Sparrow, Eichhorn & Gregg 2004), and here the proportionality $\delta_c(s) \propto \delta_m(s)$ is exact. Furthermore, similarity solutions to the Prandtl equations reveal how these boundary-layer thicknesses vary along the body, $\delta_c(s) \propto \delta_m(s) \propto \sqrt{s/U(s)}$ (Schlichting & Gersten 2000; Sparrow *et al.* 2004). The solute flux is inversely proportional to δ_c, and so for uniform flux we require that δ_c is independent of s, giving $U(s) \propto s$. Stagnation flow on a flat wall satisfies this condition and, indeed, this result helps to explain the flat nose of figure 2(*c,d*). More generally, the boundary-layer equations depend on the geometry only through the outer flow, and so any body with $U(s) \propto s$ along its front will dissolve uniformly. In particular, this condition provides a way to find shape-preserving finite bodies, where it becomes important to consider the effect of flow separation.

While the complexity of three-dimensional separated flows usually precludes analytical techniques, progress can be made in two dimensions through the use of free-streamline theory (FST). In this model, free streamlines emanate from the body and enclose a stagnant wake, outside of which the flow is ideal (inviscid and irrotational) and can thus be represented by an analytic function $u - \mathrm{i}v = U_0 \exp(-\mathrm{i}\Omega)$ (Hureau, Brunon & Legallais 1996; Moore *et al.* 2013). Here, $\Omega = \phi + \mathrm{i}\psi$ is the log-hodograph variable, where ϕ and ψ represent the flow direction and speed respectively. This flow and the paths of the free streamlines must be determined

https://doi.org/10.1017/jfm.2014.718 Published online by Cambridge University Press

simultaneously, and most often FST is used as a numerical method to calculate the flow around a known shape. Here, however, we seek to find a body that dissolves uniformly by imposing $U(s) \propto s$, thus placing a boundary condition on the flow speed. Surprisingly, FST is particularly well suited for this inverse problem, which will allow us to obtain an analytical expression for the terminal geometry.

To begin, we conformally map the flow domain to the interior of the upper half-disk (Moore *et al.* 2013). The surface of the body maps to the half-disk perimeter, $z = \exp(\mathrm{i}\theta)$, via

$$\frac{\mathrm{d}s}{\mathrm{d}\theta} = \frac{1}{2} s_0 \, |\sin 2\theta| \exp(-\psi), \tag{4.1}$$

where s_0 is the distance to separation. It should be noticed that this map depends on ψ directly. In the classical problem of flow past a given shape, only the flow direction, ϕ, is known along the boundary and thus the conformal map must be determined iteratively. Here, however, we seek a geometry that satisfies $U(s) \propto s$ along its front surface, thus placing boundary conditions on ψ and rendering (4.1) explicit. In this sense, the inverse problem is actually simpler than the direct problem. In addition to (4.1), the free streamlines map to the real segment, $z \in [-1, 1]$, with the boundary condition $U = U_0$, which results from the assumption of a stagnant wake (Moore *et al.* 2013).

In the mapped domain, the boundary conditions become

$$\psi(z) = \log|\cos\theta| \quad \text{for } z = \exp(\mathrm{i}\theta), \theta \in [0, \pi], \tag{4.2}$$

$$\psi(z) = 0 \quad \text{for } z \in [-1, 1]. \tag{4.3}$$

These conditions form a Riemann–Hilbert problem for $\Omega = \phi + \mathrm{i}\psi$ (Fokas & Ablowitz 2003), which can be solved exactly using techniques of complex analysis (to be reported separately). By evaluating the flow direction, ϕ, on the boundary, we obtain the surface tangent angle of the terminal geometry as

$$\phi = \pi/2 - (\mathrm{Li}_2(\hat{s}) - \mathrm{Li}_2(-\hat{s}))/\pi. \tag{4.4}$$

Here, $\hat{s} = s/s_0 \in [0, 1]$ is the arc length scaled on the distance to separation, and $\mathrm{Li}_2(\hat{s}) = \sum_{k=1}^{\infty} \hat{s}^k/k^2$ is the polylogarithm of second order. We show this geometry in figure 5(*a*), where we also indicate the flow streamlines as computed by FST. As seen in the figure, the terminal shape is similar to a circular arc, with nearly constant curvature along the front. Furthermore, (4.4) predicts that the flow will separate at an angle of precisely 45° with the horizontal. While this analytical solution does not address the body's back, it suggests that, for sufficiently high *Re* and *Sc*, the terminal shape is independent of scale and system parameters, such as material diffusivity or flow speed.

The predicted front surface from our 2D theory can be qualitatively compared with the 3D experiments by fitting circles to the interfaces of figure 2(*c,d*). In figure 5(*b*), we overlay the terminal shapes and the fit, showing that the front surfaces indeed have nearly constant curvature. The approach to this shape can be further quantified by measuring the front aspect ratio, as defined in the inset of figure 5(*c*). Interestingly, the sphere and cylinder data sets approach a similar value from above and below respectively, offering evidence that this final shape is a stable attractor for a broad basin of initial geometries.

We note that, strictly speaking, a uniform dissolution rate does not imply shape preservation for bodies with variable curvature. Rather, variations in curvature must

https://doi.org/10.1017/jfm.2014.718 Published online by Cambridge University Press

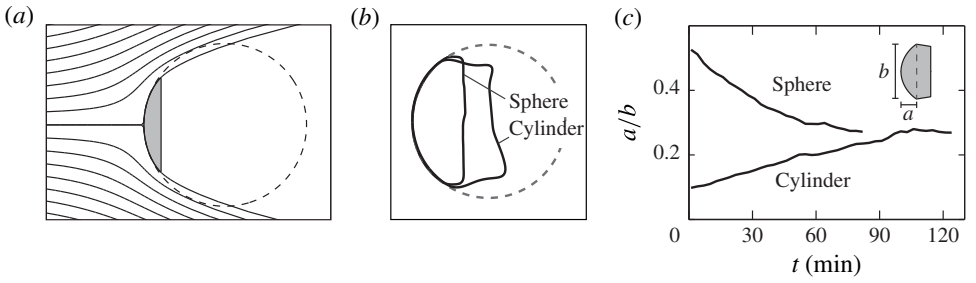


FIGURE 5. The terminal shape of a dissolving body. (*a*) Two-dimensional FST predicts a shape of nearly constant curvature along its front. (*b*) Fitting a circle to the late-time experimental interfaces also reveals fronts of nearly constant curvature for initial shapes of a sphere and an axially aligned cylinder. (*c*) The frontal aspect ratios of these two initial conditions converge to similar terminal values.

be balanced by variations in the interface velocity, as given by (A32) of Moore *et al.* (2013). However, the nearly constant curvature of the body described by (4.4), as well as the qualitative agreement with the experiments, justifies the use of uniform flux as an approximate working condition.

5. Discussion

Although not addressed by our theory, the experiments show that the body develops a surprisingly flat back. This feature might be related to the rapid mixing of solute that occurs in the body's wake. With sufficient mixing, the coarse-scale concentration might homogenize across the width of the wake while decaying in the downstream direction, thus creating a gradient aligned with the flow. Any curved surface immersed in such a field would experience non-uniform flux and thus change shape, but a flat surface would recede uniformly. These ideas could be tested using direct numerical simulations that resolve the wake flow. Simulations may also explain why our arguments based on attached boundary layers give a good account of the shrinkage of the entire body, even though significant dissolution occurs in the separated flow region of the rear. Because the typical wake flow speed is set by the imposed speed, it may be that local boundary layers in the back obey similar scaling laws.

The central principle at work during flow-driven dissolution seems to be progression towards a state of uniform material flux. This result can be intuited by considering the effect of local surface perturbations. For example, a protrusion is expected to thin the boundary layer, increasing the concentration gradient, which increases the dissolution rate and causes the perturbation to retreat. In light of this shape–flow feedback, it is interesting to compare dissolution with other moving boundary problems, such as erosion. Hydrodynamic erosion is dictated by fluid shear stress that acts to remove surface particles, and recent work from our group shows that the terminal state involves a wedge-like (2D) or conical (3D) front surface that retreats uniformly (Ristroph *et al.* 2012; Moore *et al.* 2013). The different terminal shapes for dissolution and erosion reflect different physical mechanisms at work. However, both proceed to a state of uniform material removal rate, suggesting a principle that may apply even more generally, such as during melting (Hao & Tao 2002), corrosion (Heitz 1991) and ablation (Feldman 1959; Verniani 1961).

For melting in particular, the recession rate of the interface is proportional to the heat flux (Vanier & Tien 1970), and hence uniform thermal boundary-layer thickness

https://doi.org/10.1017/jfm.2014.718 Published online by Cambridge University Press

would serve as a condition for self-similar evolution. Interestingly, experiments (Hao & Tao 2002) on ice melting in flow bear a close resemblance to ours, including the formation of a rounded front and flattened back, as well as an accelerating interface velocity. Unlike dissolution, melting can be influenced by conduction within the solid and latent heat associated with the phase transition. Furthermore, for ice melting in water, the Prandtl number is of order one, indicating that the thermal boundary layer may not be well confined within the momentum layer. It is possible that different scaling laws may apply in this regime.

Finally, the case considered here represents an intermediate case between the two well-studied extremes of dissolution in stagnant fluid and in highly agitated flows. In the absence of flow, diffusion alone acts and dissolution proceeds slowly (Garner & Suckling 1958; Garner & Hoffman 1961; Levich 1962; Duda & Vrentas 1971). In mixed flows, it is assumed that diffusion occurs across a layer near the body, although the factors that determine its thickness are typically determined empirically (Noyes & Whitney 1897; Garner & Keey 1958; Linton & Sutherland 1960; Steinberger & Treybal 1960; Levich 1962; Nelson & Shah 1975; Grijseels *et al.* 1981; Missel *et al.* 2004). Our work links dissolution directly to hydrodynamics, an approach that allows for estimation based only on the relevant scales. For example, flow of speed U_0 over a body of size a yields a recession velocity of $v_n \sim D/\delta_c \sim Sc^{1/3}D\sqrt{U_0/\nu a}$. As a whimsical application, this scaling allows us to address the following long-standing question: 'How many licks does it take to get to the centre of a lollipop?' For candy of size $a \sim 1$ cm licked at speed $U_0 \sim 1$ cm s^{-1}, we estimate a total of $U_0/v_n \sim 1000$ licks, a prediction that is notoriously difficult to test experimentally.

Acknowledgements

The authors thank M. Shelley, J. Zhang, S. Childress, M. Davies Wykes and H. Masoud for useful discussions, and the DOE (DE-FG02-88ER25053) for support.

References

BAI, G. E. & ARMENANTE, P. M. 2009 Hydrodynamic, mass transfer, and dissolution effects induced by tablet location during dissolution testing. *J. Pharm. Sci.* **98** (4), 1511–1531.

BLUMBERG, P. N. & CURL, R. L. 1974 Experimental and theoretical studies of dissolution roughness. *J. Fluid Mech.* **65** (04), 735–751.

CHILDRESS, S. 2009 *An Introduction to Theoretical Fluid Mechanics*, Courant Lecture Notes in Mathematics, vol. 19. Courant Institute of Mathematical Sciences. AMS.

COLOMBANI, J. 2008 Measurement of the pure dissolution rate constant of a mineral in water. *Geochim. Cosmochim. Acta* **72** (23), 5634–5640.

DACCORD, G. 1987 Chemical dissolution of a porous medium by a reactive fluid. *Phys. Rev. Lett.* **58** (5), 479–482.

DACCORD, G. & LENORMAND, R. 1987 Fractal patterns from chemical dissolution. *Nature* **325** (6099), 41–43.

DOKOUMETZIDIS, A. & MACHERAS, P. 2006 A century of dissolution research: from Noyes and Whitney to the biopharmaceutics classification system. *Intl J. Pharm.* **321** (1), 1–11.

DUDA, J. L. & VRENTAS, J. S. 1971 Heat or mass transfer-controlled dissolution of an isolated sphere. *Intl J. Heat Mass Transfer* **14** (3), 395–407.

FELDMAN, S. 1959 On the instability theory of the melted surface of an ablating body when entering the atmosphere. *J. Fluid Mech.* **6** (01), 131–155.

FOKAS, A. S. & ABLOWITZ, M. J. 2003 *Complex Variables: Introduction and Applications*. Cambridge University Press.

FORD, D. C. & WILLIAMS, P. W. 2007 *Karst Hydrogeology and Geomorphology*. John Wiley & Sons.

https://doi.org/10.1017/jfm.2014.718 Published online by Cambridge University Press

GARNER, F. H. & GRAFTON, R. W. 1954 Mass transfer in fluid flow from a solid sphere. *Proc. R. Soc. Lond.* A **224** (1156), 64–82.

GARNER, F. H. & HOFFMAN, J. M. 1961 Mass transfer from single solid spheres by free convection. *AIChE J.* **7** (1), 148–152.

GARNER, F. H. & KEEY, R. B. 1958 Mass-transfer from single solid spheres I: transfer at low Reynolds numbers. *Chem. Engng Sci.* **9** (2), 119–129.

GARNER, F. H. & SUCKLING, R. D. 1958 Mass transfer from a soluble solid sphere. *AIChE J.* **4** (1), 114–124.

GRIJSEELS, H., CROMMELIN, D. J. A. & DE BLAEY, C. J. 1981 Hydrodynamic approach to dissolution rate. *Pharm. Weekbl.* **3** (1), 1005–1020.

HANRATTY, T. J. 1981 Stability of surfaces that are dissolving or being formed by convective diffusion. *Annu. Rev. Fluid Mech.* **13** (1), 231–252.

HAO, Y. L. & TAO, Y.-X. 2002 Heat transfer characteristics of melting ice spheres under forced and mixed convection. *J. Heat Transfer* **124** (5), 891–903.

HEITZ, E. 1991 Chemo-mechanical effects of flow on corrosion. *Corrosion* **47** (2), 135–145.

HUREAU, J., BRUNON, E. & LEGALLAIS, P. 1996 Ideal free streamline flow over a curved obstacle. *J. Comput. Appl. Maths* **72** (1), 193–214.

JESCHKE, A. A., VOSBECK, K. & DREYBRODT, W. 2001 Surface controlled dissolution rates of gypsum in aqueous solutions exhibit nonlinear dissolution kinetics. *Geochim. Cosmochim. Acta* **65** (1), 27–34.

LEVICH, V. G. 1962 *Physicochemical Hydrodynamics*. Prentice-Hall.

LINTON, M. & SUTHERLAND, K. L. 1960 Transfer from a sphere into a fluid in laminar flow. *Chem. Engng Sci.* **12** (3), 214–229.

MAHMOOD, T. & MERKIN, J. H. 1988 Similarity solutions in axisymmetric mixed-convection boundary-layer flow. *J. Engng Maths* **22** (1), 73–92.

MBOGORO, M. M., SNOWDEN, M. E., EDWARDS, M. A., PERUFFO, M. & UNWIN, P. R. 2011 Intrinsic kinetics of gypsum and calcium sulfate anhydrite dissolution: surface selective studies under hydrodynamic control and the effect of additives. *J. Phys. Chem.* **115** (20), 10147–10154.

MEAKIN, P. & JAMTVEIT, B. 2010 Geological pattern formation by growth and dissolution in aqueous systems. *Proc. R. Soc. Lond.* A **466** (2115), 659–694.

MISSEL, P. J., STEVENS, L. E. & MAUGER, J. W. 2004 Reexamination of convective diffusion/drug dissolution in a laminar flow channel: accurate prediction of dissolution rate. *Pharmaceut. Res.* **21** (12), 2300–2306.

MOORE, M. N. J., RISTROPH, L., CHILDRESS, S., ZHANG, J. & SHELLEY, M. J. 2013 Self-similar evolution of a body eroding in a fluid flow. *Phys. Fluids* **25** (11), 116602.

NELSON, K. G. & SHAH, A. C. 1975 Convective diffusion model for a transport-controlled dissolution rate process. *J. Pharm. Sci.* **64** (4), 610–614.

NOYES, A. A. & WHITNEY, W. R. 1897 The rate of solution of solid substances in their own solutions. *J. Am. Chem. Soc.* **19** (12), 930–934.

RISTROPH, L., MOORE, M. N. J., CHILDRESS, S., SHELLEY, M. J. & ZHANG, J. 2012 Sculpting of an erodible body by flowing water. *Proc. Natl Acad. Sci. USA* **109** (48), 19606–19609.

SCHLICHTING, H. & GERSTEN, K. 2000 *Boundary-Layer Theory*. Springer.

SPARROW, E., EICHHORN, R. & GREGG, J. 2004 Combined forced and free convection in a boundary layer flow. *Phys. Fluids* **2** (3), 319–328.

STEINBERGER, R. L. & TREYBAL, R. E. 1960 Mass transfer from a solid soluble sphere to a flowing liquid stream. *AIChE J.* **6** (2), 227–232.

VANIER, C. R. & TIEN, C. 1970 Free convection melting of ice spheres. *AIChE J.* **16** (1), 76–82.

VERNIANI, F. 1961 On meteor ablation in the atmosphere. *Il Nuovo Cimento* **19** (3), 415–442.

https://doi.org/10.1017/jfm.2014.718 Published online by Cambridge University Press